Experimental study and mass transfer modelling for extractive desulfurization of diesel with ionic liquid in microreactors

Jin, Nan; Yue, Jun; Zhao, Yuchao; Lü, Hongying; Wang, Chengxiu

Published in:
Chemical Engineering Journal

DOI:
10.1016/j.cej.2020.127419

Publication date:
2021

Chemical Engineering Journal 413 (2021) 127419

Contents lists available at ScienceDirect

Chemical Engineering Journal

journal homepage: www.elsevier.com/locate/cej

Experimental study and mass transfer modelling for extractive desulfurization of diesel with ionic liquid in microreactors

Nan Jin [a], Jun Yue [b], Yuchao Zhao [a,*], Hongying Lü [a], Chengxiu Wang [c]

[a] Shandong Collaborative Innovation Center of Light Hydrocarbon Transformation and Utilization, College of Chemistry and Chemical Engineering, Yantai University, Yantai 264005, China
[b] Department of Chemical Engineering, Engineering and Technology Institute Groningen, University of Groningen, Nijenborgh 4, 9747 AG Groningen, the Netherlands
[c] State Key Laboratory of Heavy Oil Processing, College of Chemical Engineering and Environment, China University of Petroleum, Beijing 102249, China

ARTICLE INFO

Keywords:
Ionic liquids
Extractive desulfurization
Microreactor
Two-phase flow
Mass transfer

ABSTRACT

Conventional hydrodesulfurization technology was limited to treat aromatic heterocyclic sulfur compounds in ultralow-sulfur diesel. Extractive desulfurization (EDS) using ionic liquid (IL) exhibited good performance to address these issues, except for its long extraction time (15–40 min). To address this, microreactor was adopted to intensify the IL-based EDS, where dibenzothiophene was extracted from model diesel (MD) as the continuous phase to 1-butyl-3-methylimidazolium tetrafluoroborate as the dispersed phase under segmented flow (which appeared preferably at capillary numbers lower than 0.01). The effects of temperature, residence time and flow rate ratio on the desulfurization efficiency were investigated. The extraction equilibration time could be shortened from more than 15 min in conventional batch extractors to 120 s in microreactors. The extraction process was modeled according to the two-film model applied within a unit cell of the segmented flow, where the mass transfer resistance was considered primarily on the film side of the IL droplet. The mechanism for the improved EDS performance at higher temperatures or larger IL to MD flow ratios was investigated and validated, which was related to the significant increase in the diffusion coefficient or the specific interfacial area. These findings may shed important insights into the precise manipulation of IL-based EDS for a better process design and reactor optimization.

1. Introduction

To cope with the ever-stringent environmental regulations for limiting the sulfur content of diesel to 15 ppm in USA and 10 ppm in EU, Japan, and China, the deep desulfurization of diesel has become a major task all over the world [1]. Currently, hydrodesulfurization (HDS) over Co-Mo or Ni-Mo catalysts is widely employed in the refinery industries to convert effectively aliphatic sulfur compounds into H_2S [2–4], however, it is less efficient for aromatic heterocyclic sulfur compounds such as dibenzothiophene (DBT) and its derivatives [5].

To accomplish the deep desulfurization of diesel, various potential methods have been proposed and investigated as a supplement of HDS, including e.g., adsorption, oxidation, extraction and bio-desulfurization [6–11]. Among these techniques, the extractive desulfurization (EDS) has drawn more attention due to its mild operating conditions without the need of using catalysts or adsorbents [1,12–14]. Moreover, it does not change the chemical structures of other components, and the extracted sulfur compounds (after recovery) can be recycled as raw materials. Considering the environmental friendliness of chemical processes, ionic liquid (IL) was often adopted as a preferable extractant because of its low volatility, high thermal stability, tunable extracting capability and non-flammability compared to conventional organic solvents [15]. Sulfur-loaded ILs can be regenerated easily by distillation, during which sulfur compounds in the vicinity of the solvent molecules are released. After regeneration, the original structures of ILs are mostly unchanged, hence ILs are recycled without a noticeable decline in efficiency [10,12].

Many studies have been performed on IL-based EDS process, where the operating conditions, IL species and multiple-stage extractions were studied or optimized for effectively extracting aromatic sulfur compounds from fuel oils [10,14,16,17]. As early as 2001, Bösmann et al. [18] evaluated the extraction of DBT from *n*-dodecane by IL and achieved 10–30 wt% desulfurization efficiency in single-stage extraction. The DBT removal was improved to 60–70 wt% through increasing the mass ratio of IL to model diesel by Zhao et al. [16], and further to 90 wt

* Corresponding author.
E-mail address: yczhao@ytu.edu.cn (Y. Zhao).

https://doi.org/10.1016/j.cej.2020.127419
Received 21 June 2020; Received in revised form 22 September 2020; Accepted 15 October 2020
Available online 23 October 2020
1385-8947/

Nomenclature

a_i	specific interfacial area based on the MD phase volume, m^2/m^3
A	interfacial area between MD and IL phase in a unit cell, m^2
[DBT]	concentration of DBT, mol/m^3
Ca	capillary number
d	internal diameter of the microchannel, m
D	diffusion coefficient of DBT, m^2/s
K_d	distribution coefficient
L	length of segment, m
N_{DBT}	mole number of DBT, mol
Q	volumetric flow rate, m^3/s
$-R_{DBT}$	overall extraction rate of DBT, mol/s
Re	Reynolds number
T	extraction temperature, °C
u	superficial velocity, m/s
V	volume of segment, m^3
W	mass transfer rate of DBT, mol/s
X	desulfurization efficiency, %

Greek letters

α	model parameter representing mass transfer resistance, s
β	model parameter
γ	interfacial tension, N/m
δ	film thickness, m
μ	viscosity, Pa·s
ρ	density, kg/m^3
τ	residence time, s

Subscripts

c	continuous phase
d	dispersed phase
IL	IL phase
MD	MD phase
t	total

Superscripts

0	at initial state
eq	at equilibrium state
i	on the interface between MD and IL phase
wall	near the microchannel wall

% by a consecutive four-stage extraction. However, one of the acknowledged drawbacks of IL is its high viscosity slowing down the species diffusion rate [19], which usually leads to low mass transfer rate and with that, long extraction time (e.g., 15–40 min when performed in conventional extractors) [10].

An effective way to enhance the mass transfer rate is to increase the interfacial area between phases, which is exactly one of the most prominent characteristics of microreactor technology. Particularly when operating under segmented flow pattern, where both phases are present as discrete segments (i.e., droplets and slugs) with sub-millimeter scale in the miniaturized and confined space, microreactors offer not only large interfacial area and short diffusion distance, but also additional internal circulation that is critical for further enhancing mixing and mass transfer [20–23]. Previous studies on using ILs or other highly viscous liquids (e.g. deep eutectic solvents, polymers.) for extraction processes have proved the superiority of the segmented flow microreactor compared with the conventional extraction equipment [24–28]. Tsaoulidis et al. [24] carried out the extraction of dioxouranium (VI) from nitric acid solutions by TBP/[Bmim][NTf_2] mixtures in a microchannel of 0.5 mm internal diameter. By dispersing the nitric acid solution as plugs, the extraction of dioxouranium (VI) reached more than 85% of the equilibrium value within 15 s, and the overall volumetric mass transfer coefficient was found in a range of 0.049 to 0.312 s^{-1}, which is much higher than that of conventional contactors (generally $< 10^{-2}\,s^{-1}$) [29]. An increase of the IL to aqueous phase flow ratio, which led to a larger specific interfacial area, is helpful to increase the rate of mass transfer. Liu et al. [26] used [Bmim][PF_6] as the continuous slugs to extract butanone oxime from the aqueous ammonium sulfate solution in a microchannel, where the equilibrium state was achieved in a residence time of 50 s, while it took 20 min in batch experiments. It was further found that decreasing the inner diameter of the microchannel from 1 mm to 0.75 mm improved the extraction efficiency by 10%, because the resulted decrease of slug size and increase of specific surface area improved the mass transfer. Recently, Al-Azzawi et al. [28] compared the EDS performance of polyethylene glycol and a deep eutectic solvent in miniaturized borosilicate channels of different diameters, and further confirmed the presence of higher percentage of extraction when using a small diameter channel. It was also concluded that the time for reaching the equilibrium was reduced in microchannel devices by almost 99% of that in conventional batch processes. In addition, the higher viscosity of the deep eutectic solvent was found to decrease the mixing efficiency, leading to a longer equilibrium time than that in the case of using polyethylene glycol as the extractant.

Realizing a precise process control is another advantage of microreactor technology, which allows for a reliable interpretation of mass transfer property and an improved product quality. Taking advantage of well-defined interfacial area in segmented flow, Kamio et al. [30,31] developed a kinetic model to investigate the extraction dynamics of docosahexaenoic acid ethyl ester. The fast extraction equilibrium by the segmented flow processing in the microreactor was considered due to the large specific interfacial area of the slug facilitated by the presence of wall film and the thin mass transfer boundary layer caused by the internal circulation. In the continuous production of 5-hydroxymethylfurfural (HMF) in microreactors, Shimanouchi et al. [32] obtained a higher yield and selectivity of HMF in the segmented flow microreactor than those for conventional approaches, and concluded that the mass transfer of HMF across the interface was enhanced by the vortex field generated in the segmented flow.

All these efforts demonstrated to some extent the intensification potential of microreactor technology in multiphase systems. Inspired by these researches, applying microreactor operation into IL-based EDS process is expected to offer a promising solution to circumvent the negative effect of low mass transfer rate in IL (especially when using conventional extractors) and in the meantime to provide an in-depth understanding of the process. Despite a few application studies of IL-based extraction in microreactors, the knowledge concerning flow and mass transfer properties of IL-involved systems in microreactors is rather scarce, but important for a rational design of microreactors and the chemical process optimization. Therefore, the current study is concerned with an experimental study of IL-based EDS process in a microreactor, where DBT was extracted from model diesel (MD) by 1-butyl-3-methylimidazolium tetrafluoroborate ([Bmim][BF_4]). The flow characteristics of the MD-IL system was investigated firstly to obtain a desirable segmented flow, under which the effect of varying microchannel length (i.e., residence time), extraction temperature and flow ratio on the EDS performance was explored. Based on the flow and EDS results, the mass transfer resistances were then modelled and discussed, from which the underlying mechanism about how the operating conditions affect the EDS performance was elaborated. The findings of this work may be useful for guiding the operation of not only EDS, but also other liquid–liquid extraction processes (such as nuclear extraction, solute enrichment for sample analysis and bio-molecules extraction) in

microreactors.

2. Experimental section

2.1. Materials

n-Octane (Sinopharm Chemical Reagent Co., Ltd) with DBT (Shanghai Aladdin Bio-Chem Technology Co., Ltd) at selected concentrations were used as MD with a sulfur content of 500 ppm, where *n*-tetradecane (Sinopharm Chemical Reagent Co., Ltd) was added (at a concentration of 2000 ppm) as the internal standard. 1-Butyl-3-methylimidazolium tetrafluoroborate ([Bmim][BF_4]; Lanzhou Institute of Chemical Physics, Chinese Academy of Sciences) was selected as the representative IL extractant [10,16,22]. Physical properties of these fluids are listed in Table 1.

2.2. Experimental setup

The hydrodynamic experimental set up for MD-IL system is depicted in Fig. 1. It consisted of two syringe pumps (Longer LSP01-1A, 5 μm/min-65 mm/min line velocity, ±0.5% accuracy) equipped with two glass syringes (10 mL, 14.7 mm internal diameter), a microreactor section and a product collector (2 mL centrifuge tube). The details of the microreactor section are shown in the inset of the figure, in which three circular fluorinated ethylene propylene (FEP) microchannels (508 μm internal diameter, IDEX Health & Science) were connected by an ethylene-tetra-fluoro-ethylene (ETFE) T-type connector (508 μm internal bore diameter, IDEX Health & Science). MD and IL phases were introduced into the respective inlet microchannels by the syringe pumps, mixed at the T-type connector, and flowed through the outlet microchannel to the collector. A high-speed CCD video camera (Phantom R311, 24–650000 fps frame rate, 1280 × 800 pixels, 20 μm pixel size) connected to a stereo microscope (Olympus SZX16, 2.1x-690x magnification, 16.4x zoom) was employed to record two-phase flow patterns in the microchannel at a speed of 300–3200 fps. The visualization zone of interest was at the location about 50, 60 and 70 cm from the T-type connector. Before recording the flow patterns, the system was running for at least 5 min to ensure the establishment of a stable flow. In each series of experiments, the IL to MD volumetric ratio (Q_{IL}/Q_{MD}) varied from 0.1 to 0.5 and Q_{IL} from 40 μL/min to 700 μL/min. All experiments were performed at ambient temperature and pressure.

To reveal the EDS performance, additional experiments were conducted in a temperature-controlled microreactor system, as presented in Fig. 2. The microreactor section was arranged in a helical shape immersed into a heating bath (Julabo CD200F, −20–150 °C temperature-controlled range, ±0.1 °C accuracy), allowing the extraction to be conducted at varying temperatures from 30 °C to 70 °C. The residence time was varied from 4 s to 120 s by adjusting the length of the extraction microchannel from 200 cm to 1200 cm (i.e., the length to diameter ratio of 3939–23622). At the extraction microchannel outlet, samples were quickly cooled in an ice-water bath (~0 °C) to terminate the extraction process. The effective quenching at the outlet collector (i.e., the centrifuge tube) was verified by the extremely low desulfurization efficiency (<2%) when conducting the extraction experiments in the centrifuge tube at the temperature of 0 °C and the residence time of 40 s (corresponding to the maximum sample collecting time). Thus, the mass transfer end effect is considered negligible compared with the extraction contribution in the microreactor section, except for the cases with low desulfurization efficiency at short residence time. Besides, the current method is convenient to use, though the online phase separation, e.g., as used in the work of Susanti et al. [35], represents a better option (the functioning of which at various temperature levels still needs to be tested). After separation, the desulfurized MD sample was collected and analyzed. All tests were repeated at least twice to ensure a favorable repeatability and accuracy of the system.

Table 1
Physical properties of the used working fluids.

Temperature (°C)	Model diesel (MD) [a]		[Bmim][BF_4] [b]		Interfacial tension [c] (mN/m)
	Density (g/cm^3)	Viscosity (mPa·s)	Density (g/cm^3)	Viscosity (mPa·s)	
25	0.703	0.508	1.201	108	15.38
30	0.698	0.480	1.198	84.6	15.34
40	0.690	0.431	1.191	53.5	15.26
50	0.682	0.389	1.184	35.6	15.17
60	0.673	0.352	1.176	25.2	15.09
70	0.665	0.321	1.169	18.0	15.00

[a] Approximated by properties of *n*-octane, obtained from the manufacturer, since adding such small amounts of DBT (as sulfur compound) and *n*-tetradecane (as internal standard) had little effect on the property change.
[b] Obtained from the literature [33,34].
[c] Between IL and MD; measured by a tensiometer (Biolin Sigma 700, see more details in Section 2.3).

2.3. Analytics

The Agilent 7890A gas chromatography (GC), equipped with a flame ionization detector and an automatic sampler, was employed to analyze the DBT concentration in the MD feed as well as that in the desulfurized MD after extraction in the microreactor. GC conditions were as follows: inlet temperature at 250 °C, detector temperature at 250 °C, and oven temperature program consisting of a heating process with a ramp of 15 °C/min from 100 °C to 200 °C, followed by an isothermal step at 200 °C for 4 min. All samples were analyzed at least twice, and the relative error was found within ± 2%.

The Biolin Sigma 700 tensiometer, equipped with a temperature-controlled jacket, allowed to measure interfacial tension at different temperatures. The interfacial tension values between IL and MD phases were measured using pendant drop method with the experimental standard deviation no more than 3%.

2.4. Definitions

To quantify the EDS performance, the desulfurization efficiency (X) and the distribution coefficient (K_d) are defined as the following.

$$X = \frac{[\mathrm{DBT}]^0_{\mathrm{MD}} - [\mathrm{DBT}]_{\mathrm{MD}}}{[\mathrm{DBT}]^0_{\mathrm{MD}}} \times 100\% \quad (1)$$

$$K_d = \frac{[\mathrm{DBT}]^{eq}_{\mathrm{IL}}}{[\mathrm{DBT}]^{eq}_{\mathrm{MD}}} \quad (2)$$

where $[\mathrm{DBT}]^0_{\mathrm{MD}}$ and $[\mathrm{DBT}]_{\mathrm{MD}}$ are the concentrations of DBT in the MD phase before and after extraction, respectively; $[\mathrm{DBT}]^{eq}_{\mathrm{MD}}$ and $[\mathrm{DBT}]^{eq}_{\mathrm{IL}}$ are the equilibrium concentrations of DBT in the MD and IL phases, respectively.

3. Results and discussion

3.1. Flow characteristics of MD-IL system in the microchannel

A stable MD-IL segmented flow in the microchannel is essential to quantify the mass transfer properties and regulate the EDS process. Manipulation of flow pattern has been extensively studied for the regular oil–water system [36,37], while the knowledge concerning IL-involved system is rather scarce, especially when viscous IL serves as the dispersed phase. The flow characteristics of MD-IL system were investigated on the visualization experimental setup (Fig. 1). Considering the high cost of IL limits its large-scale application, Q_{IL}/Q_{MD} in the present work was set as 0.1–0.5, lower than that in the batch EDS experiments (generally 0.2–2). The Q_{IL} and Q_{MD} varied in the range of 40–700 μL/min and 80–7000 μL/min, respectively, preventing the

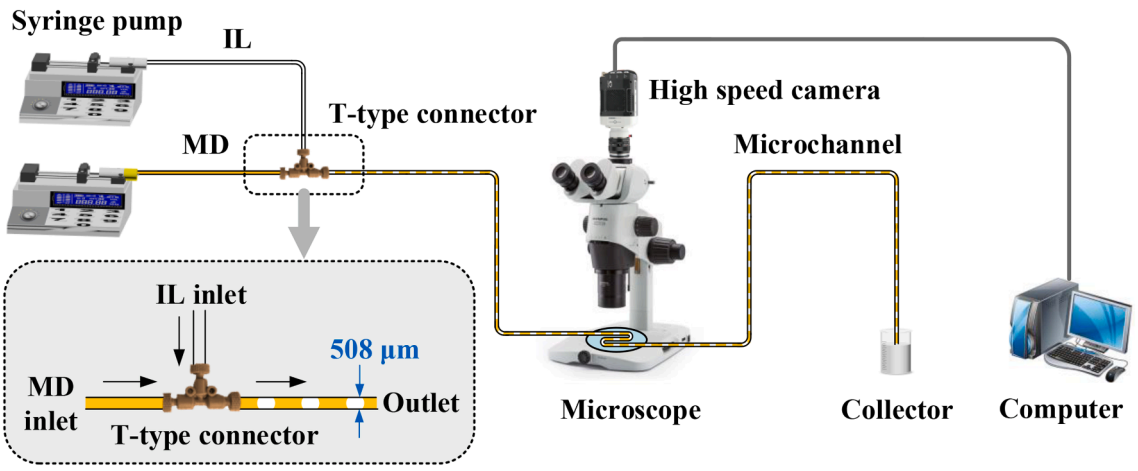

Fig. 1. Schematic diagram of the visualization experimental setup.

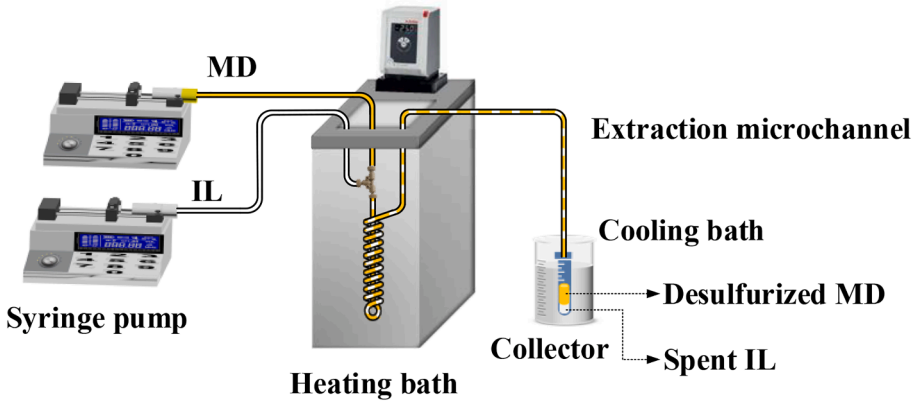

Fig. 2. Schematic diagram of the EDS experimental setup.

occurrence of unstable flow at too small or too high flow rates.

3.1.1. Flow patterns

As the wettability of MD on the FEP microchannel wall is stronger than that of IL, MD appeared as the continuous phase. When decreasing Q_{IL}/Q_{MD}, three flow patterns were observed in our experiments: the slug flow, the cobble flow, and the droplet flow (Fig. 3). Their characteristics are summarized as follows:

(1) The slug flow mainly happened at high Q_{IL}/Q_{MD} values (e.g., Q_{IL}/Q_{MD} greater than 0.33). Herein, the convex-shaped IL plug was dispersed in the continuous MD phase and had a longer axial length (L_{IL}) than the microchannel diameter (d). The MD phase is separated into slugs that are connected with each other by the wall film lubricating the plug body.

(2) The cobble flow occurred as Q_{IL}/Q_{MD} decreased to around 0.25. In this situation, the IL phase appeared as cobbles with smaller axial lengths than the microchannel diameter, but comparable radial dimensions to the microchannel diameter.

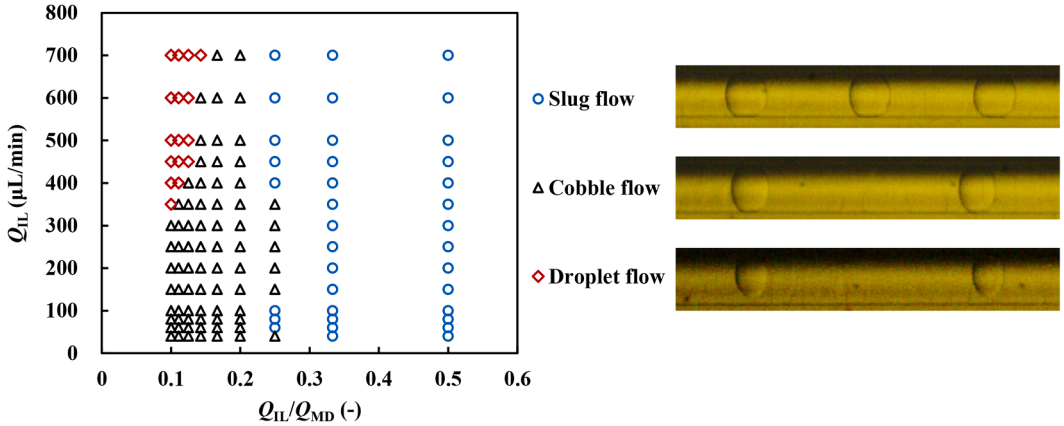

Fig. 3. Typical flow patterns observed for MD-IL system in a FEP microchannel.

(3) The droplet flow appeared in systems with relatively high Q_{IL} values and the low Q_{IL}/Q_{MD} ratio (e.g., Q_{IL} greater than 400 μL/min and $Q_{IL}/Q_{MD} < 0.15$). The radial and axial lengths of the IL droplets were both less than the microchannel diameter, just as the IL droplets were suspended in the MD phase. Unfortunately, the droplet flow was often unstable, in which the sizes of IL bubbles as well as MD slugs became nonuniform.

Generally, the existence of two-phase flow patterns in microchannels depends on the competition of the shear force (exerted on the dispersed phase by the continuous phase) with the interfacial tension [36]. When involving the fluid with a high viscosity and density, the viscous and inertial forces become important. Therefore, inspired by the previous studies [22], a division of the flow pattern was made based on the capillary number of the continuous phase ($Ca_c = \frac{\mu_c u_c}{\gamma}$) and Reynolds number of the dispersed phase ($Re_d = \frac{du_d\rho_d}{\mu_d}$). As shown in Fig. 4, three distinguished zones are identified as follows:

(1) The interfacial tension dominated zone: when Ca_c was relatively low at a given Re_d, the interfacial tension was large enough to dominate over the shear force. The incipient IL phase blocked the cross sectional area of the channel completely before it was cut off by the continuous MD phase, so the two-phase flow tended to form the slug flow [38].
(2) The transition zone: as Ca_c increased, the shear force gradually contributed to the droplet breakup together with the interfacial tension, so IL formed the cobble-like droplets smaller than the above plugs [38]. It is noticeable that Re_d affected the transition from the interfacial force dominated zone to the transient zone greatly in the present study. At higher Re_d, the inertial force of dispersed phase started to participate but played a resistive role in the droplet formation process. This necessitated a stronger shear force to form smaller bubbles, which corresponded to a higher critical Ca_c.
(3) The viscous force dominated zone: when Ca_c exceeded 10^{-2}, a critical value above which the shear stress started to dominate the breakup process, the two-phase flow behaved as the droplet flow.

Compared with the flow pattern map of the *n*-heptane-[Emim][$EtSO_4$] system in the work of Scheiff et al. [39], the present work obtained a similar trend but slightly smaller critical Ca_c values for the transition line between the interfacial force dominated zone and the transient zone. Such shift can be explained by that the viscosity of [Bmim][BF_4] is slightly higher that [Emim][$EtSO_4$], and the operation window of slug flow would be narrowed if the viscosity of the dispersed phase was increased [39]. For the toluene-[Bmim][BF_4] and ethanol-silicone oil systems in the work of Bai et al. [38], the effect of Re_d on the transition from the interfacial force dominated zone to the transient zone was not evident, probably due to the small flow rate range of the dispersed phase (3–20 μL/min). Despite that, the orders of magnitude of the critical Ca_c values for the two transition lines (corresponding to 10^{-3} and 10^{-2}, respectively) aligned fairly well.

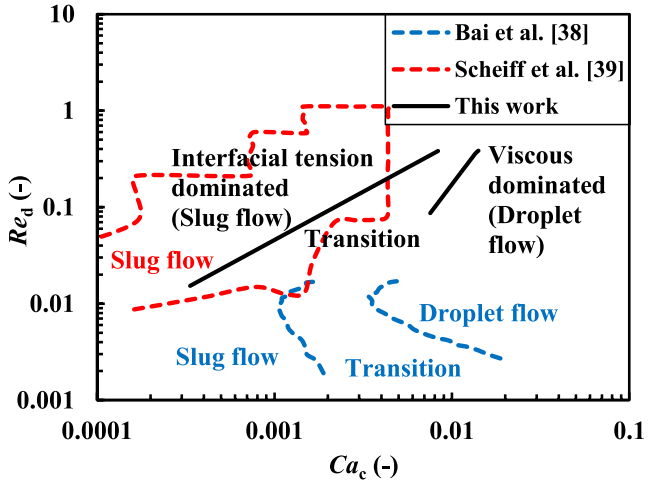

Fig. 4. Flow pattern map of MD-IL system and other reported IL-dispersed systems in the microchannel based on dimensionless parameters.

Among the various flow patterns, the segmented flow (including slug and cobble flow) received our preference for carrying out EDS due to its good flow controllability, broad window of operation and well-defined interfacial areas. Therefore, in the following sections, the EDS experiments were conducted and the results presented are in the segmented flow zone, which is dominant at lower Ca_c numbers (e.g. $Ca_c < 0.01$).

3.1.2. Segment lengths

Segment size is one of the important parameters for the manipulation of dispersed flow and estimation of mass transfer property. In the current experiments, the segment lengths were measured from microscope images (Section 2.2). All the segment lengths were averaged over a set of 30 images. At each set of flow conditions, the segment lengths were quite consistent, which had low values of standard deviation (below 2%).

Fig. 5 shows the effect of phasic flow rates on the normalized length of IL segment (L_{IL}/d). These variations can be explained by the force analysis during its formation process. The length of the dispersed IL segment in the microchannel is governed mainly by the competition between forces that have a negative effect (i.e., shear force exerted on the IL phase by the MD phase, viscous force of IL phase) and forces that have a positive effect (i.e., interfacial tension at the interface of two phases, inertial force of the IL phase) [38,40]. Increasing Q_{MD} (i.e., the superficial velocity of MD phase, u_{MD}) makes the shear force ($\sim\mu_{MD}u_{MD}$) on the IL phase larger and thereby L_{IL} smaller (Fig. 5(b)). The increase of Q_{IL} (i.e., the superficial velocity of IL phase, u_{IL}) improves both the inertial force ($\sim d\rho_{IL}u_{IL}^2$) of IL and its viscous force ($\sim\mu_{IL}u_{IL}$), but the increase amplitude of the former is greater than the latter, therefore L_{IL}/d still increases (Fig. 5(a-b)). When fixing the total mixture flow rate (Q_t), L_{IL}/d showed a linear relationship with Q_{IL}/Q_{MD} in Fig. 5(c), as a result of decreasing Q_{MD} and increasing Q_{IL} simultaneously [41].

A complicated relationship between L_{IL}/d and Q_t was found at a constant flow ratio (Fig. 5(d)).When Q_t is relatively low (e.g. < 500 μL/min), the role of shear force and interfacial tension dominates in the resulted L_{IL}/d. The increase of Q_t leads to a larger shear force and thereby a lower L_{IL}/d (Fig. 5(d)). As Q_t increased to more than 500 μL/min, the viscous and inertial forces of IL phase increased gradually and began to affect L_{IL}/d together with the shear force. Although all these forces increased with Q_t, the increase amplitude of inertial force was greater than other forces because it was proportional to the square of the velocity. Especially at higher Q_{IL}/Q_{MD}, the contrast became more evident. Therefore, L_{IL}/d increased with Q_t at higher Q_t and Q_{IL}/Q_{MD} (e.g., Q_t greater than 500 μL/min and Q_{IL}/Q_{MD} greater than 0.2). On the other hand, when Q_{IL}/Q_{MD} is sufficiently small (e.g., $Q_{IL}/Q_{MD} < 0.2$), the IL velocity is so low compared with the MD velocity that the inertial force of IL phase is not dominant over the shearing force of MD, hence L_{IL}/d still decreased at higher Q_t.

To predict the segment size in microchannels, some models have been developed, either empirically or from the segment formation mechanism, in which the segment size was correlated with the phase ratio and/or capillary numbers [42,43]. However, the liquid viscosity also affects the segment size [44,45], some related parameters (e.g., *Re* or μ of the highly viscous fluid) were then taken into consideration, as shown in the models listed in Table 2.

Fig. 6. Comparison of normalized IL lengths between the experimental data and the modelled values with Eq. (3) and several correlations from the literatures.

Inspired by the literatures [22,41,44], the segment size is described

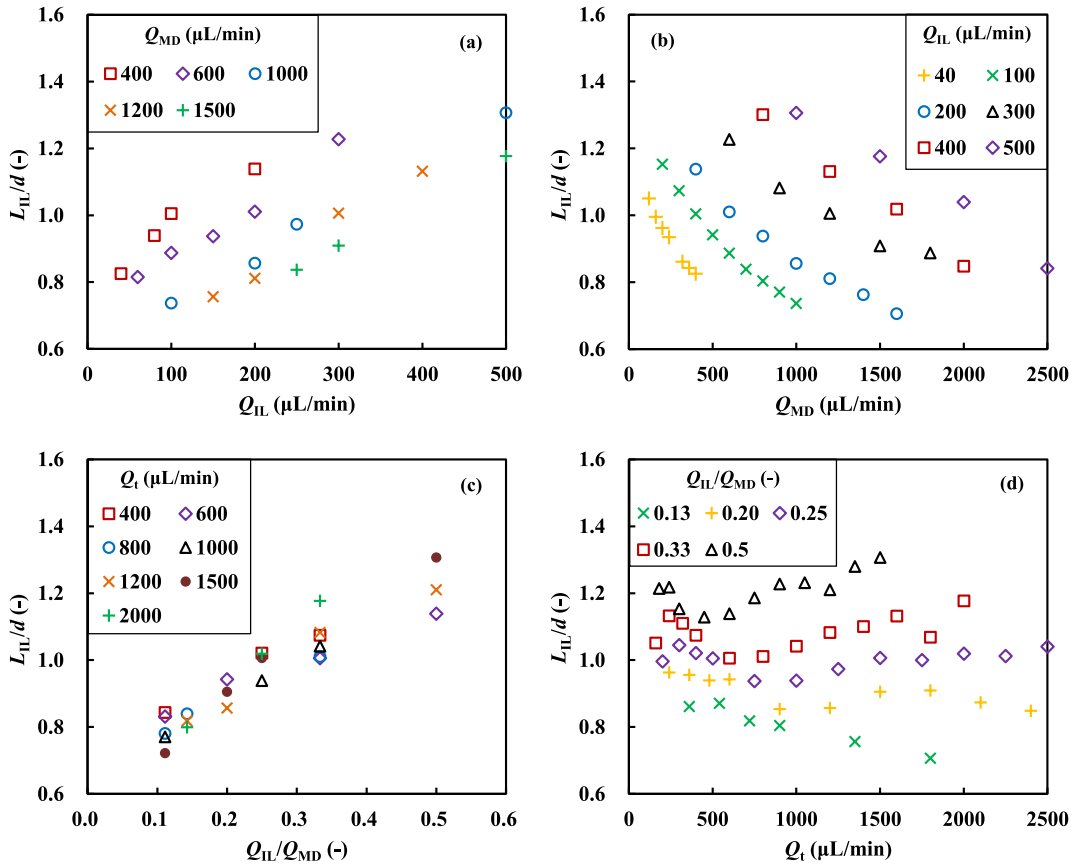

Fig. 5. Variation of normalized IL lengths (L_{IL}/d) against flow rates.

Table 2
Several correlations of normalized segment size for flow of highly viscous systems in microchannels.

Correlation	Conditions	Reference
$\frac{L}{d} = 0.23\mu_c^{0.10}Ca^{-0.31}$	Continuous fluid: tolueneDispersed fluid: [Bmim][BF_4]Channel: square (height/width: 500 μm)Conditions: Re_d = 0.002–0.02, $Ca_c = 10^{-5}$-0.02	Bai et al. [38]
$\frac{L}{d} = 0.768(Ca^*)^{-0.24}\left(\frac{u_d}{u_c}\right)^{0.194}$ $Ca^* = \frac{(\varphi_c\mu_c + \varphi_d\mu_d)u_c}{\gamma}$	Continuous fluid: keroseneDispersed fluid: glycerol aqueous solutionChannel: square (height/width: 500 μm) Conditions: Re_d = 0.08–3.5, $Ca_c = 10^{-6}$-10^{-5}	Su et al. [44]
$\frac{L}{d} = 2.2882Ca^{-0.2728}Re^{0.4617}Re_c^{-0.9634}$ [a]	Continuous fluid: TBP/[Bmim][NTf_2]Dispersed fluid: HNO_3 solutionChannel: circular (d = 0.5, 1, 2 mm)Conditions: Re_d = 0.13–0.30, Ca_c = 0.01–0.09	Tsaoulidis et al. [41]

[a] The Ca exponent is 0.2728 in the original article, which seems to be a misprint, because L/d showed a negative relation with Ca in their experimental results. Hence, a negative value was used here.

as a function of Ca_{MD} and Re_{IL}, as given below

$$\frac{L_{IL}}{d} = 0.3354Ca_{MD}^{-0.2777}Re_{IL}^{0.2728} \quad (3)$$

The exponent of Ca_{MD} is −0.2777, in good accordance with the previous studies (Table 2). The absolute values of exponents for Ca_{MD} and Re_{IL} are approximately equal, indicating that the properties of the dispersed phase are as important as that of the continuous phase in the present work. Based on Eq. (3), the predicted L_{IL}/d under all stable operating conditions agreed well with the experimental data, and the relative error was lower than 10% (Fig. 6).

Compared with L_{IL}/d, the normalized MD slug length (L_{MD}/d) varies in a quite wide range of 1.0–6.0, which increased with Q_{MD} and decreased with Q_{IL}. When Q_t was constant, L_{MD}/d seems to decrease exponentially with increasing Q_{IL}/Q_{MD}. The detailed data are presented in the supplementary material (Fig. S1).

On the other hand, the MD segment was formed synchronously with the IL segment, the ratio of their lengths (L_{IL}/L_{MD}) should be thus a function of Q_{IL}/Q_{MD} as well. When the droplets are long enough (so the cap length is negligible) and the wall film between the IL and the microchannel is neglected, it can be assumed that the IL droplet velocity (u_{IL}) is equal to the mixture velocity (u_t) and $L_{IL}/L_{MD} \approx Q_{IL}/Q_{MD}$. In the current work, the volumes of the two caps and the wall film accounted for 3–8% of the volume of a unit cell (consisting of one IL and one MD segment), so the correlation turns out to be

$$\frac{L_{IL}}{L_{MD}} = 1.4432\frac{Q_{IL}}{Q_{MD}} \quad (4)$$

by correlating the experimental data of L_{IL}/L_{MD} with Q_{IL}/Q_{MD} (Fig. 7). Similar relations was found with the coefficient of 1.49 in a gas–liquid system [45]. The relative error of the proposed correlation is within ± 10% for predicting the measured length of continuous MD slug.

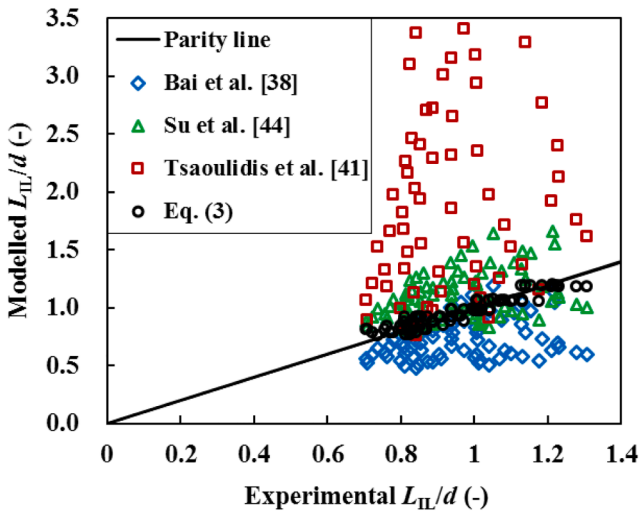

Fig. 6. compares the predicted results for our experimental data by the models in Table 2. The first two correlations predicted better than the last one, because the highly viscous fluid acted as the dispersed phase both in our and the first two studies [38,44], while it served as the continuous phase in the work of Tsaoulidis et al. [41]. In addition, the operating conditions and the channel geometry are also important factors that influence the forces exerted on the dispersed phase in the formation process as mentioned earlier, and then the segment lengths. In the current work, the operating conditions (Re_d = 0.005–0.35, Ca_c = 10^{-5}-10^{-2}) were varied in wider ranges than that in the literatures, leading to that the suggested models cannot describe our experimental data satisfactorily. (For interpretation of the references to colour in this figure legend, the reader is referred to the web version of this article.)

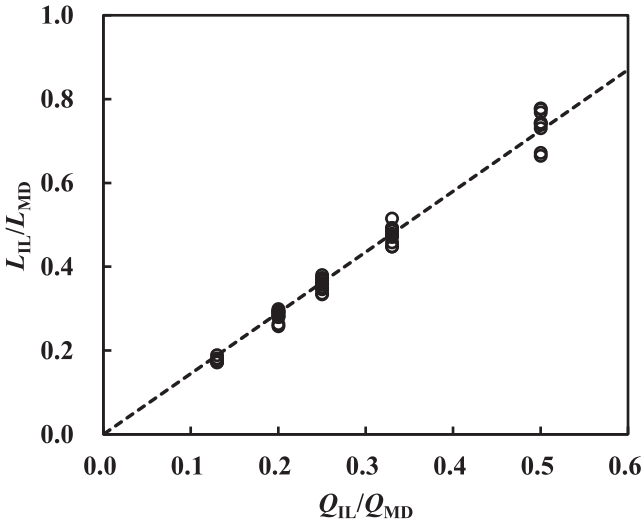

Fig. 7. Variation of normalized MD lengths (L_{IL}/d) against flow rate ratios.

3.2. Desulfurization performance of IL-based EDS in the microchannel

In the segmented flow zone (Ca_{MD} < 0.01; cf. Fig. 4), the desulfurization performance of IL-based EDS in the microchannel was evaluated. Referred to the previous studies, the extraction temperature was set at 30–70 °C to pursue a balance between IL viscosity, energy consumption and desulfurization efficiency. The flow rate ratio (Q_{IL}/Q_{MD}) remained in the range of 0.1–0.5, consistent with the conditions used in the hydrodynamic experiments. The residence time was controlled by adjusting the length of the microchannel. After overall consideration of the two factors, Q_t was fixed at 1215 μL/min, and the residence time varied from 4 s to 120 s. Within the operating window, the effects of the temperature (T), the flow rate ratio (Q_{IL}/Q_{MD}) and the residence time (τ) on the desulfurization efficiency (X) were investigated.

Fig. 8(a-c) display the desulfurization efficiency as a function of the residence time under different conditions. As increasing the residence time, the desulfurization efficiency increased firstly and then gradually leveled off, indicating that the extraction equilibrium was almost achieved within 120 s. For the cases with the temperature being 30 °C and Q_{IL}/Q_{MD} being 0.1 and 0.2, the residence time was further extended to 300 s to confirm that the equilibrium time is around 120 s (not detailed here, see Fig. S2 for supplementary material). In contrast, only 90% of the equilibrium efficiency was obtained at the batch time of 30 min when employing a glass flask for the extraction, either for volume ratio of 0.1 with temperature of 70 °C, or for volume ratio of 0.5 with temperature of 30 °C (detailed results in Fig. S3 for supplementary material). Even when increasing the IL to MD volume ratio to 1, more than 15 min were still needed to reach equilibrium in this batch operation no matter using [Bmim][BF_4] [46] or other ILs (e.g. [Pmim][Tf_2N], [Bmim][SCN]) [10,16] as extractants. This illustrates the superiority of microreactors in conducting IL-based EDS process.

Based on the results of Fig. 8(a-c), the equilibrium efficiency for the removal of DBT (X^{eq}) could be estimated and summarized in Fig. 8(d). Moreover, the distribution coefficients (K_d) were calculated by Eq. (2) based on the equilibrium concentrations of DBT in both phases and tabulated in Table 3. It is evident that the elevated temperature and Q_{IL}/Q_{MD} ratio are favorable for desulfurization. An increase in the Q_{IL}/Q_{MD} ratio corresponds to an increase in the interfacial area, which means IL and DBT had more opportunities to contact with each other, leading to a high sulfur removal. Comparing with Q_{IL}/Q_{MD}, the desulfurization efficiency is not very sensitive to the temperature variation. The slight increase of the desulfurization efficiency with temperature rise (Fig. 8 (d)) may be originated from the decrease of the IL viscosity, which makes DBT more prone to diffuse to IL and as a result, a higher desulfurization efficiency.

Summarizing the effects of operating conditions on the desulfurization efficiency, an optimal EDS condition in the microchannel was suggested as: an extraction temperature of 50–60 °C to balance the IL viscosity and energy consumption, an IL to MD volume ratio of 0.5 to balance the desulfurization efficiency and production cost, a residence time of 60 s to balance the desulfurization efficiency and microreactor capacity.

3.3. Modelling the microfluidic IL-based EDS process based on mass transfer rates

To gain a deep understanding on the microfluidic IL-based EDS process, the fundamental mass transfer characteristics deserve to be studied. Among various mass transfer models, two-film model was chosen to describe our system, based on three important considerations: (1) Albeit its simplicity, two-film theory can usually provide similar conclusions to those of more advanced mass transfer models such as Higbies' penetration model and Danckwerts's surface renewal theory [47]; (2) EDS is operated under segmented flow in the laminar regime, hence the interface renewal is believed relatively slow; (3) Two-film model is commonly used in the literature for modelling extraction in microreactor systems and has shown good agreement to the experimental data [30–32,48].

Specifically, mass transfer in EDS could be divided into three steps, as shown in Fig. 9: (1) the diffusion of DBT from the bulk MD phase to the interface across the MD film, (2) the equilibrium distribution of DBT at the two-phase interface, and (3) the diffusion of DBT from the interface to the bulk IL phase across the IL film. The mass transfer resistance is considered to concentrate in the MD and IL films, so their thicknesses are two important parameters, which are closely related to the flow topology inside the segments. It is reported that the internal circulation was fully developed in the continuous segment, while only accounted for 30–75% of the dispersed segment [39,49]. Therefore, as shown in Fig. 9,

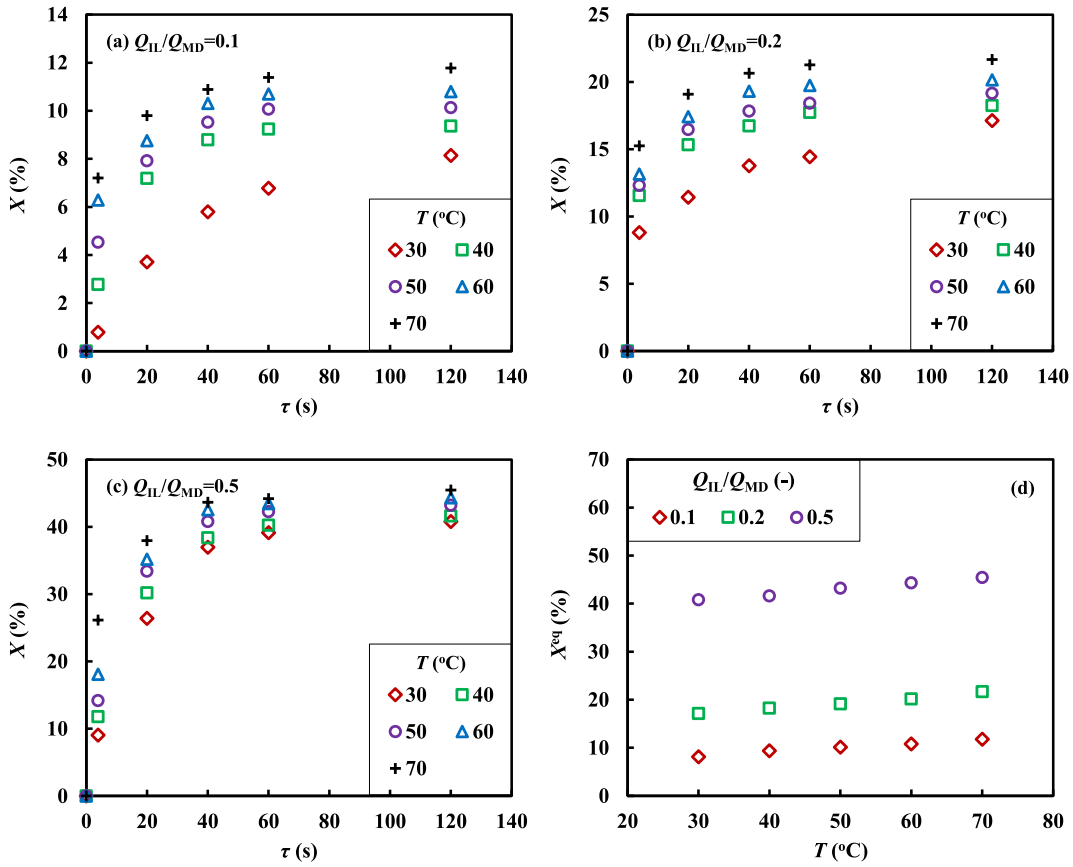

Fig. 8. Temporal variations of the desulfurization efficiency (Q_t = 1215 μL/min, d = 508 μm).

Table 3
Distribution coefficients (K_d) of DBT between MD to IL phase. [a]

Q_{IL}/Q_{MD} (-)	Temperature (°C)				
	30	40	50	60	70
0.1	0.8863	1.0330	1.1277	1.2105	1.3351
0.2	1.0338	1.1162	1.1845	1.2623	1.3830
0.5	1.3780	1.4248	1.5216	1.5924	1.6666

[a] Conditions: Q_t = 1215 μL/min, d = 508 μm, τ = 120 s.

the thickness of the MD film (δ_{MD}) is assumed less than that of the wall film (δ_{MD}^{wall}), i.e., $0 \le \delta_{MD} \le \delta_{MD}^{wall}$.

The mass transfer rate of DBT from the bulk MD to the interface through the MD film, W_{MD}, is expressed as

$$W_{MD} = \frac{AD_{MD}}{\delta_{MD}}\left([DBT]_{MD} - [DBT]_{MD}^{i}\right) \quad 5$$

where δ_{MD} is the thickness of the hypothetical MD film; D_{MD} is the diffusion coefficient of DBT in the MD phase; $[DBT]_{MD}$ and $[DBT]_{MD}^{i}$ are the concentrations of DBT in the bulk MD phase and on the MD film-side interface, respectively; A is the interfacial area between phases.

The mass transfer rate from the interface to the bulk IL, W_{IL}, is derived

$$W_{IL} = \frac{AD_{IL}}{\delta_{IL}}\left([DBT]_{IL}^{i} - [DBT]_{IL}\right) \quad (6)$$

where δ_{IL} is the thickness of the hypothetical IL film; D_{IL} is the diffusion coefficient of DBT in the IL phase; $[DBT]_{IL}$and $[DBT]_{IL}^{i}$ are the concentrations of DBT in the bulk IL phase and on the IL film-side interface, respectively.

The concentration of DBT near the interface is in thermodynamic equilibrium,

$$K_d = \frac{[DBT]_{IL}^{eq}}{[DBT]_{MD}^{eq}} = \frac{[DBT]_{IL}^{i}}{[DBT]_{MD}^{i}} \quad (7)$$

At steady state, $W_{MD} = W_{IL}$ and both are equal to the overall extraction rate of DBT ($-R_{DBT}$). Thus, it is obtained that

$$-R_{DBT} = \frac{[DBT]_{MD} - \frac{[DBT]_{IL}}{K_d}}{\frac{\delta_{MD}}{AD_{MD}} + \frac{1}{K_d}\cdot\frac{\delta_{IL}}{AD_{IL}}} \quad 8$$

According to the mass balance, the concentrations of DBT satisfy the following expression.

$$[DBT]_{IL} = \left([DBT]_{MD}^{0} - [DBT]_{MD}\right)\frac{V_{MD}}{V_{IL}} \quad (9)$$

where V_{MD} and V_{IL} are the volume of MD slug and that of IL droplet in a unit cell, respectively; $[DBT]_{MD}^{0}$ is the initial concentration of DBT in the bulk MD phase.

Substituting Eq. (9) into Eq. (8), $-R_{DBT}$ is expressed as

$$-R_{DBT} = \frac{[DBT]_{MD} - \frac{1}{K_d}\cdot\frac{V_{MD}}{V_{IL}}\left([DBT]_{MD}^{0} - [DBT]_{MD}\right)}{\frac{\delta_{MD}}{AD_{MD}} + \frac{1}{K_d}\cdot\frac{\delta_{IL}}{AD_{IL}}} \quad 10$$

It is known that $-R_{DBT}$ is defined as

$$-R_{DBT} = \frac{dN_{DBT}}{d\tau} = -V_{MD}\frac{d[DBT]_{MD}}{d\tau} \quad 11$$

where N_{DBT} is the number of moles of DBT and τ is the residence time.

Combining Eq. (10) and Eq. (11), it is finally obtained that

$$-\frac{d[DBT]_{MD}}{d\tau} = \frac{(1+\beta)[DBT]_{MD} - \beta[DBT]_{MD}^{0}}{\alpha} \quad (12)$$

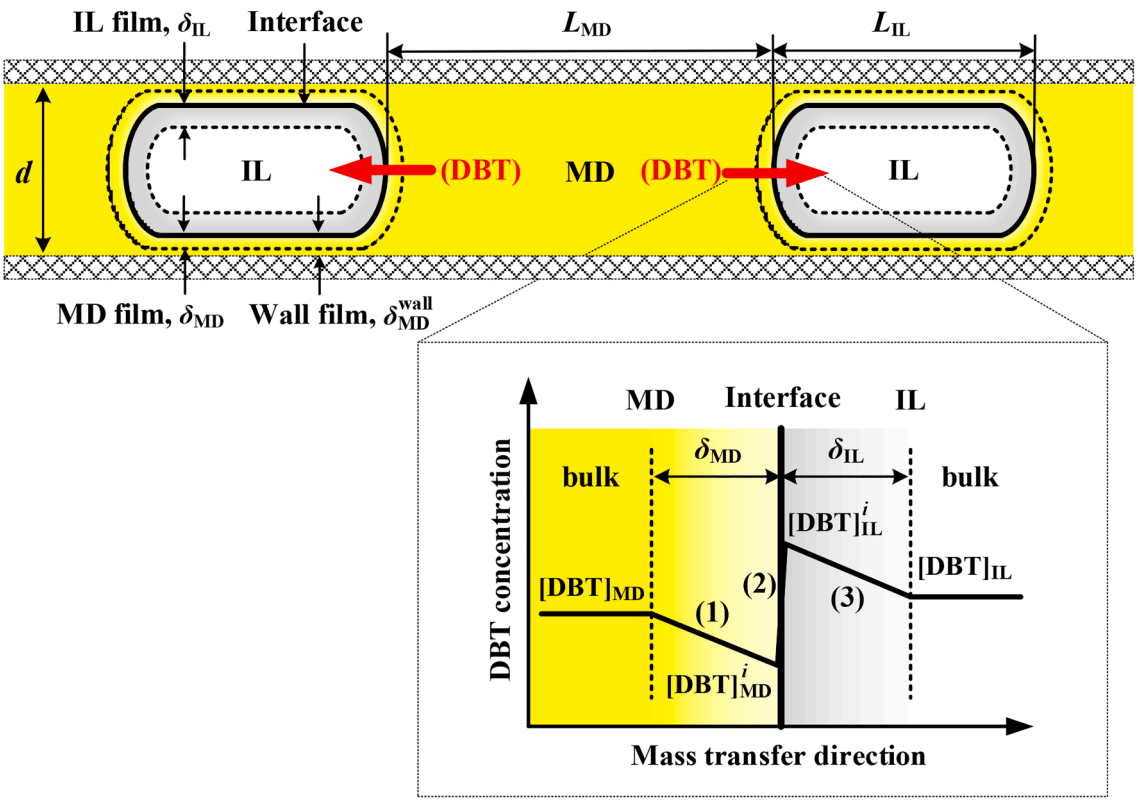

Fig. 9. Simplified mass transfer scheme under segmented flow of MD-IL system in the microchannel.

where

$$\alpha = \frac{\delta_{MD} V_{MD}}{A D_{MD}} + \frac{1}{K_d}\cdot\frac{\delta_{IL} V_{MD}}{A D_{IL}} = \frac{\delta_{MD}}{a_i D_{MD}} + \frac{1}{K_d}\cdot\frac{\delta_{IL}}{a_i D_{IL}} \quad (13)$$

and

$$\beta = \frac{1}{K_d}\cdot\frac{V_{MD}}{V_{IL}} \quad (14)$$

In Eq. (13), a_i is the specific interfacial area based on the volume of MD slug.

Integrating Eq. (12) with the initial condition of $[DBT]_{MD} = [DBT]_{MD}^{0}$ at $\tau = 0$, the DBT concentration in the bulk MD phase along the microchannel is derived as

$$[DBT]_{MD} = [DBT]_{MD}^{0}\frac{\beta + e^{-\frac{1+\beta}{\alpha}\tau}}{1+\beta} \quad (15)$$

With the modelled $[DBT]_{MD}$ value, the desulfurization efficiency (X) can be estimated as

$$X = \frac{1 - e^{-\frac{1+\beta}{\alpha}\tau}}{1+\beta} \quad (16)$$

Based on the flow characteristics and extraction behavior, the EDS process in the microchannel could be modelled according to Eq. (16). A combination of the predicted results and the experimental results can give important insights into the EDS process, such as the rate-controlling step and the underlying mechanism about how the operating conditions affect the EDS performance.

3.3.1. Effect of the film thickness on EDS

Taking the extraction process at a Q_{IL}/Q_{MD} of 0.5 and a temperature of 30 °C as an example (Fig. 8(c)), Table 4 summarizes the known parameters as required in the model (Eq. (16)) and the thicknesses of two films (δ_{MD} and δ_{IL}) are the only two unknown parameters. Hence, several values of δ_{MD} and δ_{IL} were attempted to model the process with Eq. (16).

Table 4
Determined model parameters at a Q_{IL}/Q_{MD} of 0.5 and a temperature of 30 °C.

Items	Values	Sources
L_{IL} ($\times 10^{-4}$ m)	6.41	Eq. (3)
L_{MD} ($\times 10^{-4}$ m)	9.11	Eq. (4)
D_{IL} ($\times 10^{-11}$ m^2/s)	1.99 [a]	Eq. (S1)
D_{MD} ($\times 10^{-9}$ m^2/s)	2.50 [a]	Eq. (S2)
V_{IL} ($\times 10^{-10}$ m^3)	1.05 [a]	Eq. (S10)
V_{MD} ($\times 10^{-10}$ m^3)	2.10 [a]	Eq. (S11)
a_i ($\times 10^{3}$ m^2/m^3)	4.31 [a]	Eq. (S12)
K_d	1.38	Table 3

[a] Detailed calculation procedure was provided in the supplementary material (Section S3).

Considering the fact that $\delta_{MD}^{wall} < 10$ μm (estimated by Eq. (S3)) in this work, the effect of δ_{MD} was discussed in a value range of 1–9 μm. As stated above, the spread scope of internal circulation in the dispersed phase (IL) was smaller than that in the continuous phase (MD) [39,49], making it reasonable to set a larger δ_{IL}. Moreover, this disparity was also aggravated by the much higher viscosity of IL. Therefore, the maximum value of IL film thickness was set as 20 μm.

Fig. 10 displays the modelling results with different δ_{MD} and δ_{IL} values. Big differences were found in the effects of δ_{MD} and δ_{IL} on the EDS process. The desulfurization efficiency curves overlapped with each other for δ_{MD} (Fig. 10(a)), whereas they are clearly separated for δ_{IL} (Fig. 10(b)). This indicates that δ_{MD} had no effect on EDS, while δ_{IL} made a great influence. In the two-film model, two terms in Eq. (13) correspond to the mass transfer resistances in MD and IL films, denoted as $\alpha_{MD} = \frac{\delta_{MD}}{a_i D_{MD}}$ and $\alpha_{IL} = \frac{1}{K_d}\cdot\frac{\delta_{IL}}{a_i D_{IL}}$, respectively. It was found from Table 5 that the mass transfer resistance in the IL film (α_{IL}) was much greater than that in the MD film (α_{MD}) by about two orders of magnitude. This is mainly resulted from the big difference between D_{MD} ($\sim 10^{-9}$ m^2/s) and D_{IL} ($\sim 10^{-11}$ m^2/s), given the much higher viscosity of IL than that of MD (Table 1). This concludes that the mass transfer resistance in this EDS

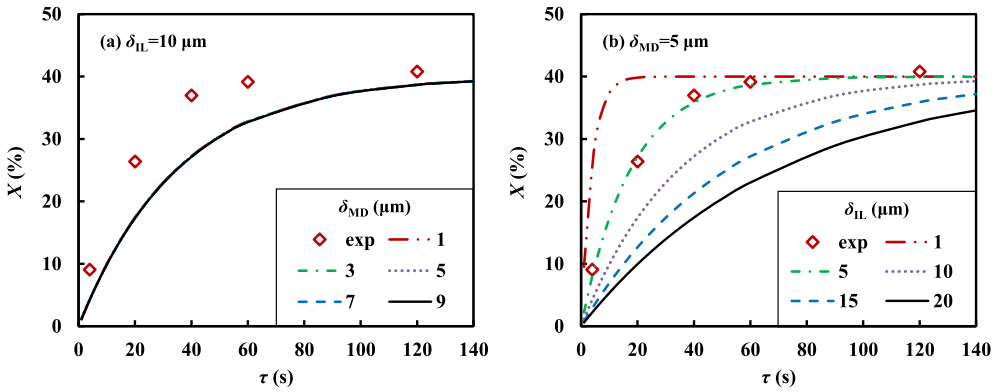

Fig. 10. Effects of film thickness on the desulfurization efficiency (T = 30 °C, Q_{IL}/Q_{MD} = 0.5).

Table 5
Mass transfer resistances in MD and IL films (T = 30 °C, Q_{IL}/Q_{MD} = 0.5).

δ_{MD}, $\times10^{-6}$ m	1	3	5	7	9
α_{MD}, s	0.09	0.28	0.46	0.65	0.84
δ_{IL}, $\times10^{-6}$ m	1	5	10	15	20
α_{IL}, s	9.20	44.14	87.81	131.49	175.16

process concentrates primarily on the IL side. Therefore, a slight change of δ_{IL} leads to a big difference in the desulfurization efficiency (Fig. 10 (b)), while changing δ_{MD} is insignificant to affect the mass transfer rate (Fig. 10(a)). By comparing the predicted and experimental results, the reasonable value of δ_{IL} was set at 5 μm for Q_{IL}/Q_{MD} of 0.5 and temperature of 30 °C for a best fitting (Fig. 10(b)). Unfortunately, the exact value of δ_{MD} cannot be obtained, but it would not affect the modelling results no matter which value is chosen. Herein, it was simply set as 5 μm under all conditions. Although these values may not be sufficiently accurate, at least it is certain that the film thickness is thinner than that of the stagnant region outside the vortex field of internal circulation.

3.3.2. *Prediction of the desulfurization efficiency*

With the same approach shown above, the known parameters in the model (Eq. (16)) at other conditions were calculated and then δ_{IL} values were fitted (not detailed here, see Table S1 for supplementary material). Based on these parameters, the desulfurization efficiencies at various conditions were predicted. Fig. 11 presents the comparison of the desulfurization efficiencies between the modelled values and the experimental data (relevant to Fig. 8). A reasonable agreement between the model predictions and the experimental results was obtained, with the relative error lower than 10% for most data. The large deviation mainly happened for the short residence time (e.g., τ < 20 s). This can be ascribed to the delayed separation after extraction, as described in Section 2.2. It still took a few seconds to separate the spent IL from the desulfurized MD completely in the collecting flask (Fig. 2). Thus, the extraction still proceeded slightly outside the microchannel, which could not be neglected (when compared with extraction in the microchannel) at much short residence time operation in the microchannel. Thus, the measured desulfurization efficiency turned out to be a little higher than the model prediction.

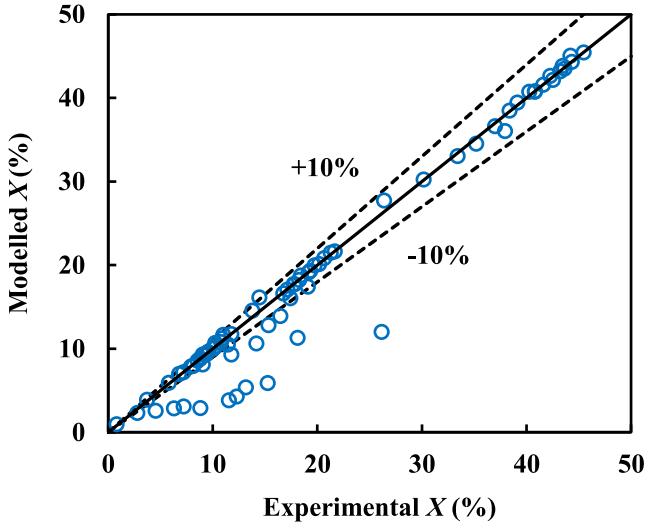

Fig. 11. Comparison of desulfurization performance between the experimental data and the modelled values by Eq. (16).

3.3.3. *Relationships between flow, mass transfer and desulfurization performance*

To further understand the IL-based EDS process in the microchannel, it is necessary to analyze the underlying mechanism into how the operating conditions affect the EDS performance. Therefore, the effects of operating conditions on flow and mass transfer were investigated according to the modelling (Fig. 12). A conclusion has been drawn from Table 5 that the mass transfer resistance (α) concentrated primarily on the IL film. Therefore, only the influencing factors of α_{IL} (i.e., δ_{IL}, K_d, D_{IL}, a_i) were discussed.

It can be seen from Fig. 12(a) that α decreased with Q_{IL}/Q_{MD} at a fixed temperature. One of the important reasons is the significant increase of the specific interfacial area (a_i) (Fig. 12(c)), which is greatly dependent on L_{IL} and L_{MD}. Increasing Q_{IL}/Q_{MD} at constant Q_t contributes to a larger L_{IL} (Fig. 5(c)) but a smaller L_{MD} (Fig. S2(c)), and accordingly a larger interfacial area (A) and smaller MD slugs (V_{MD}). These variations are responsible for an increased a_i and a decreased α. In addition, based on the fact the slug length variation affects the mass transfer rate, another important conclusion can be drawn that the contributions of the wall film and two caps to the mass transfer are both important, and the wall film tends to play a more important role at longer IL segment lengths in enhancing the overall extraction rate. This consideration is also in line with the experimental results in other studies [25,50–53].

Similar to a_i, δ_{IL} was also positively affected by Q_{IL}/Q_{MD} (Fig. 12(b)) due to the change of L_{IL}. This is mainly associated with the internal circulation in the IL segment, which has been demonstrated regarding its intensification effect on mixing and mass transfer [41,54]. For the segmented flow, evidence shows that within the bigger droplets, the recirculation is less efficient [22,41], implying δ_{IL} would become larger at increasing Q_{IL}/Q_{MD}. Besides, K_d (Table 3) were also positively correlated with Q_{IL}/Q_{MD}. More specially, with the increase of Q_{IL}/Q_{MD} from 0.1 to 0.5, a_i or K_d (the increase of which is favorable for decreasing α) was improved by a factor of 3.7 or 0.2–0.5, respectively, and δ_{IL} (the increase of which tends to increase α) was raised by ca. 50%. Thus, the negative effect of the increased δ_{IL} is counteracted by the positive effect

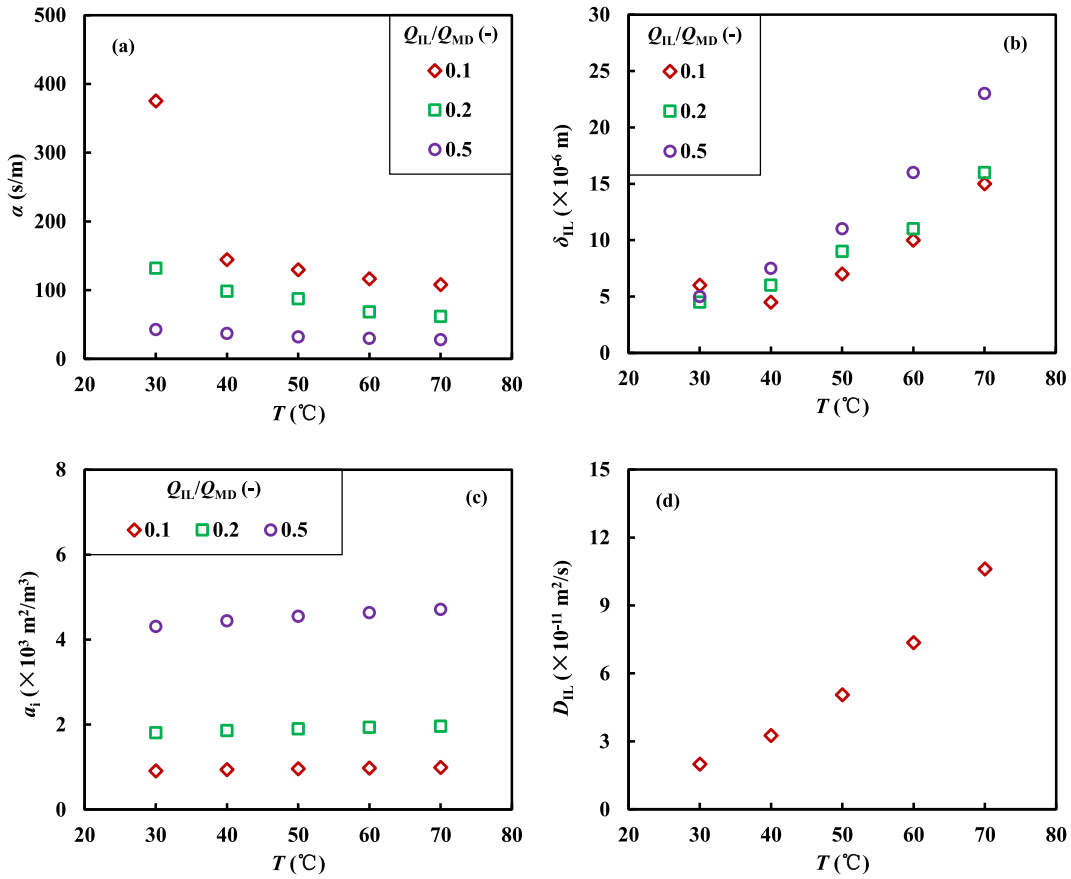

Fig. 12. Effects of operating conditions on the flow and mass transfer parameters.

of other parameters (especially by a_i), leading to a reduced α by 75%.

With respect to the extraction temperature, it influences α mainly by decreasing the viscosities for both phases, especially for the dispersed IL phase (it has a drastic viscosity reduction from 84.6 mPa·s at 30 °C to 18 mPa·s at 70 °C) (Table 1). This leads to a remarkable improvement of D_{IL} (Fig. 12(d)) based on Eq. (S1), specifically by a factor of 4.3 when elevating the temperature from 30 °C to 70 °C. On the other hand, the decreased viscosities are also responsible for the increase of L_{IL} (Eq. (3)), intrinsically due to the reduced shearing force from MD and viscous force of IL. As explained before, a larger L_{IL} is accompanied by a greater δ_{IL}, hence a 1.5–3.6 fold increase occurred in δ_{IL} (Fig. 12(b)). Synchronously with L_{IL}, L_{MD} was increased as well at a fixed Q_{IL}/Q_{MD} (Eq. (4)), leading to that a_i remained nearly constant (Fig. 12(c)). In addition, K_d had a slight increase to be 20–50% higher (Table 3). When all of these parameters are considered together, α declined to 30–65% of the original value, under which circumstances the adverse effect of δ_{IL} is mainly compensated by D_{IL}. In addition, it is noteworthy from Fig. 12(a) that the sensitivity of α to the temperature was weakened with the increase of Q_{IL}/Q_{MD}, which also explains why the EDS performance became less affected by the temperature at Q_{IL}/Q_{MD} of 0.5 (Fig. 8). For Q_{IL}/Q_{MD} of 0.5, a_i is at such a high value that the variations of other parameters played a minor effect. This suggests that the specific interfacial area plays a dominant role in the mass transfer of EDS process, which is consistent with the observation that increasing the IL-to-MD ratio is more effective than elevating the temperature towards an improved EDS performance (Fig. 8).

As indicated in the discussion above, the interfacial mass transfer is coupled with the fluid convection in the slugs/droplets (mainly due to the internal circulation). In this respect, the concentration field (e.g., regarding its non-uniformity in relation to the residence time distribution (RTD) in each phase) is another important aspect needs to be well understood. For the dispersed droplet, as the interface around it is closed, it is considered as a mini ideal batch reactor, thus its RTD curve approximates to the Dirichlet function [55]. For the continuous phase, the adjacent slugs are connected by the wall film, through which the solute can move from one slug to another. Theoretically, the axial diffusion widens RTD, which can be further affected by the mass transfer due to the dynamic variation of the fluid properties or the slug lengths along the microchannel [56]. Nevertheless, it is still narrow and has little influence on the mass transfer in the present work. First of all, the extraction is conducted in a circular microchannel with small capillary numbers, the wall film is thin and the leakage flow can be negligible. Under these circumstances, the axial dispersion between slugs through the wall film is suppressed, thus RTD in the continuous phase is narrow enough. Then, the initial solute concentration was only 500 ppm, which means the total flux of mass transfer is extremely low. Further considering the incompressible nature of the MD-IL system, the changes of the slug lengths and the fluid properties during the mass transfer can be negligible, as well as RTD. Hence, the effect of mass transfer on RTD is not taken into our consideration.

Above all, the IL-based EDS process in microreactors is well described by the proposed mass transfer analysis according to the two-film model (e.g., cf. Eq. (16)), based on which an insight into this process could be recognized. The EDS performance is closely related to the flow topology and mass transfer. When altering the operating conditions (e.g., flow ratio and temperature), changes would occur in the lengths of segments, and with that the corresponding film thickness and the specific interfacial area. Coordinated with the variation of the diffusion and distribution coefficients by temperature change, the above flow parameters lead to the variations of the mass transfer resistance, and eventually, of the extraction rate. Among these parameters, increasing the specific interfacial area was found to bring the most significant effect

for decreasing the mass transfer resistance in the current work. However, the exact film thickness for mass transfer within the two-film model is not fully understood yet. Further efforts are thus needed to be address this. In addition, from the aspect of large-scale application, fundamental research on the microreactor scale-up, such as how to well handle the fluid distribution across numerous microchannels in parallel and a multitude of microreactor modules, remains to be further investigated.

4. Conclusions

To improve the extraction efficiency of the IL-based EDS process, thus achieving smaller extractor footprint and lowering IL usage/cost for potential industrial application, the segmented flow microreactor was investigated for the process. With the extractant of [Bmim][BF_4], the two-phase flow characteristics in the microchannel were investigated firstly. Three distinct flow patterns were observed, among which the segmented flow (with MD as the continuous phase and IL as the dispersed phase) appeared at $Ca_{MD} < 0.01$. By correlating with Ca_{MD} and Re_{IL} (Eq. (3)), the measured segment size could be predicted reasonably well. This equation provides a basis for estimating the segment length and the corresponding interfacial area necessary for interpreting mass transfer in EDS.

Within the operating widow of segmented flow, MD containing DBT was desulfurized in the microchannel at the temperature of 30–70 °C, Q_{IL}/Q_{MD} ratio of 0.1–0.5 and residence time of 4–120 s. The desulfurization performance increased greatly with increasing Q_{IL}/Q_{MD}, and slightly with the temperature rise. The extraction equilibrium was almost achieved within 120 s, much shorter than that in the batch operation, which exhibits advantages of the microreactor processing for process efficiency improvement.

To have a better understanding on the IL-based EDS process, the two-film model was used to describe the mass transfer rate in the microchannel, by using two characteristic film thicknesses (δ_{MD} and δ_{IL}) for mass transfer on the MD and IL sides. The developed model (Eq. (16)) using the fitted δ_{IL} value was shown to describe the measured desulfurization efficiency with an acceptable accuracy. It was found that the mass transfer resistance in this EDS process concentrated primarily on the IL film-side due to the much lower diffusion coefficient of DBT in IL than in MD. The distribution coefficient, the specific interfacial area, the IL film thickness and the diffusion coefficient of DBT in IL appeared to be the main factors responsible for the observed effect of the operating conditions on the EDS performance. When increasing the temperature or Q_{IL}/Q_{MD}, the adverse effect of an increased IL film thickness on mass transfer is counteracted by the positive contribution from other factors, eventually leading to a better desulfurization efficiency. These findings may provide useful guidelines for the design and operation of microreactors towards an improved EDS performance thereof.

Declaration of Competing Interest

The authors declare that they have no known competing financial interests or personal relationships that could have appeared to influence the work reported in this paper.

Acknowledgements

We gratefully acknowledge the financial supports from National Natural Science Foundation of China (Nos. 21808194, 21978250), Natural Science Foundation of Shandong Province (No. ZR2017BB058) and Key Technology Research and Development Program of Shandong (2019JZZY010410).

Appendix A. Supplementary data

Supplementary data to this article can be found online at https://doi.org/10.1016/j.cej.2020.127419.

References

[1] P.S. Kulkarni, C.A. Afonso, Deep desulfurization of diesel fuel using ionic liquids: current status and future challenges, Green Chem. 12 (2010) 1139–1149.
[2] Y. Zhang, W. Han, X. Long, H. Nie, Redispersion effects of citric acid on CoMo/γ-Al_2O_3 hydrodesulfurization catalysts, Catal. Commun. 82 (2016) 20–23.
[3] X. Wang, Z. Zhao, P. Zheng, Z. Chen, A. Duan, C. Xu, J. Jiao, H. Zhang, Z. Cao, B. Ge, Synthesis of NiMo catalysts supported on mesoporous Al_2O_3 with different crystal forms and superior catalytic performance for the hydrodesulfurization of dibenzothiophene and 4, 6-dimethyldibenzothiophene, J. Catal. 344 (2016) 680–691.
[4] F.J. Méndez, O.E. Franco-López, X. Bokhimi, D.A. Solís-Casados, L. Escobar-Alarcón, T.E. Klimova, Dibenzothiophene hydrodesulfurization with NiMo and CoMo catalysts supported on niobium-modified MCM-41, Appl. Catal. B 219 (2017) 479–491.
[5] R. Shafi, G.J. Hutchings, Hydrodesulfurization of hindered dibenzothiophenes: an overview, Catal. Today 59 (2000) 423–442.
[6] A.J. Hernández-Maldonado, R.T. Yang, Desulfurization of diesel fuels by adsorption via π-complexation with vapor-phase exchanged Cu(I)-Y zeolites, J. Am. Chem. Soc. 126 (2004) 992–993.
[7] J. Xiao, S. Sitamraju, Y. Chen, S. Watanabe, M. Fujii, M. Janik, C. Song, Air-promoted adsorptive desulfurization of diesel fuel over Ti-Ce mixed metal oxides, AIChE J. 61 (2015) 631–639.
[8] F. Davoodi-Dehaghani, M. Vosoughi, A.A. Ziaee, Biodesulfurization of dibenzothiophene by a newly isolated Rhodococcus erythropolis strain, Bioresour. Technol. 101 (2010) 1102–1105.
[9] Z. Ismagilov, S. Yashnik, M. Kerzhentsev, V. Parmon, A. Bourane, F. Al-Shahrani, A. Hajji, O. Koseoglu, Oxidative desulfurization of hydrocarbon fuels, Catal. Rev.: Sci. Eng. 53 (2011) 199–255.
[10] R. Abro, A.A. Abdeltawab, S.S. Al-Deyab, G. Yu, A.B. Qazi, S. Gao, X. Chen, A review of extractive desulfurization of fuel oils using ionic liquids, RSC Adv. 4 (2014) 35302–35317.
[11] H. Lu, P. Li, C. Deng, W. Ren, S. Wang, P. Liu, H. Zhang, Deep catalytic oxidative desulfurization (ODS) of dibenzothiophene (DBT) with oxalate-based deep eutectic solvents (DESs), Chem. Commun. 51 (2015) 10703–10706.
[12] Z. Ren, Z. Zhou, M. Li, F. Zhang, L. Wei, W. Liu, Deep desulfurization of fuels using imidazole anion-based ionic liquids, ACS Sustainable Chem. Eng. 7 (2018) 1890–1900.
[13] J. Gao, H. Meng, Y. Lu, H. Zhang, C. Li, A carbonium pseudo ionic liquid with excellent extractive desulfurization performance, AIChE J. 59 (2013) 948–958.
[14] Z. Song, C. Zhang, Z. Qi, T. Zhou, K. Sundmacher, Computer-aided design of ionic liquids as solvents for extractive desulfurization, AIChE J. 64 (2018) 1013–1025.
[15] S. Zhang, J. Sun, X. Zhang, J. Xin, Q. Miao, J. Wang, Ionic liquid-based green processes for energy production, Chem. Soc. Rev. 43 (2014) 7838–7869.
[16] H. Zhao, G.A. Baker, D.V. Wagle, S. Ravula, Q. Zhang, Tuning task-specific ionic liquids for the extractive desulfurization of liquid fuel, ACS Sustainable Chem. Eng. 4 (2016) 4771–4780.
[17] L.C. Player, B. Chan, M.Y. Lui, A.F. Masters, T. Maschmeyer, Toward an understanding of the forces behind extractive desulfurization of fuels with ionic liquids, ACS Sustainable Chem. Eng. 7 (2019) 4087–4093.
[18] A. Bösmann, L. Datsevich, A. Jess, A. Lauter, C. Schmitz, P. Wasserscheid, Deep desulfurization of diesel fuel by extraction with ionic liquids, Chem. Commun. (2001) 2494–2495.
[19] F. Guo, S. Zhang, J. Wang, B. Teng, T. Zhang, M. Fan, Synthesis and applications of ionic liquids in clean energy and environment: a review, Curr. Org. Chem. 19 (2015) 455–468.
[20] V. Hessel, D. Kralisch, N. Kockmann, T. Noël, Q. Wang, Novel process windows for enabling, accelerating, and uplifting flow chemistry, ChemSusChem 6 (2013) 746–789.
[21] A. Adamo, R.L. Beingessner, M. Behnam, J. Chen, T.F. Jamison, K.F. Jensen, J.-C.-M. Monbaliu, A.S. Myerson, E.M. Revalor, D.R. Snead, On-demand continuous-flow production of pharmaceuticals in a compact, reconfigurable system, Science 352 (2016) 61–67.
[22] C. Yao, Y. Zhao, G. Chen, Multiphase processes with ionic liquids in microreactors: hydrodynamics, mass transfer and applications, Chem. Eng. Sci. 189 (2018) 340–359.
[23] A. Hommes, T. De Wit, G.J.W. Euverink, J. Yue, Enzymatic biodiesel synthesis by the biphasic esterification of oleic acid and 1-butanol in microreactors, Ind. Eng. Chem. Res. 58 (2019) 15432–15444.
[24] D. Tsaoulidis, V. Dore, P. Angeli, N.V. Plechkova, K.R. Seddon, Dioxouranium (VI) extraction in microchannels using ionic liquids, Chem. Eng. J. 227 (2013) 151–157.
[25] D. Tsaoulidis, P. Angeli, Effect of channel size on mass transfer during liquid-liquid plug flow in small scale extractors, Chem. Eng. J. 262 (2015) 785–793.
[26] Y. Liu, C. Zhang, K. Wu, X. Ye, C. He, Microchannel extraction of butanone oxime from aqueous ammonium sulfate solution using ionic liquids, J. Chem. Eng. Chin. Univ. 31 (2017) 530–537.
[27] Z. Al Ani, T. Al Wahaibi, F.S. Mjalli, A. Al Hashrrri, B. Abu-Jdayil, Flow of deep eutectic solvent-simulated fuel in circular channels: part II-extraction of dibenzothiophene, Chem. Eng. Res. Des. 119 (2017) 294–300.
[28] M. Al-Azzawi, F.S. Mjalli, A. Al-Hashmi, T. Al-Wahaibi, B. Abu-jdayil, Optimal liquid fuel extractive desulfurization in micro and mini-channels, Chem. Eng. Process. 140 (2019) 43–51.

[29] Y. Zhao, G. Chen, Q. Yuan, Liquid-liquid two-phase mass transfer in the T-junction microchannels, AIChE J. 53 (2007) 3042–3053.
[30] E. Kamio, Y. Seike, H. Yoshizawa, T. Ono, Modeling of extraction behavior of docosahexaenoic acid ethyl ester by utilizing slug flow prepared by microreactor, AIChE J. 56 (2010) 2163–2172.
[31] E. Kamio, Y. Seike, H. Yoshizawa, H. Matsuyama, T. Ono, Microfluidic extraction of docosahexaenoic acid ethyl ester: comparison between slug flow and emulsion, Ind. Eng. Chem. Res. 50 (2011) 6915–6924.
[32] T. Shimanouchi, Y. Kataoka, T. Tanifuji, Y. Kimura, S. Fujioka, K. Terasaka, Chemical conversion and liquid-liquid extraction of 5-hydroxymethylfurfural from fructose by slug flow microreactor, AIChE J. 62 (2016) 2135–2143.
[33] K.R. Harris, M. Kanakubo, L.A. Woolf, Temperature and pressure dependence of the viscosity of the ionic liquid 1-butyl-3-methylimidazolium tetrafluoroborate: viscosity and density relationships in ionic liquids, J. Chem. Eng. Data 52 (2007) 2425–2430.
[34] D. Matkowska, T. Hofman, High-pressure volumetric properties of ionic liquids: 1-butyl-3-methylimidazolium tetrafluoroborate,[C_4mim][BF_4], 1-butyl-3-methylimidazolium methylsulfate [C_4mim][$MeSO_4$] and 1-ethyl-3-methylimidazolium ethylsulfate,[C_2mim][$EtSO_4$], J. Mol. Liq. 165 (2012) 161–167.
[35] J.G. Winkelman, B. Schuur, H.J. Heeres, J. Yue, Lactic acid extraction and mass transfer characteristics in slug flow capillary microreactors, Ind. Eng. Chem. Res. 55 (2016) 4691–4702.
[36] Y. Zhao, G. Chen, Q. Yuan, Liquid-liquid two-phase flow patterns in a rectangular microchannel, AIChE J. 52 (2006) 4052–4060.
[37] A.A. Yagodnitsyna, A.V. Kovalev, A.V. Bilsky, Flow patterns of immiscible liquid-liquid flow in a rectangular microchannel with T-junction, Chem. Eng. J. 303 (2016) 547–554.
[38] L. Bai, Y. Fu, S. Zhao, Y. Cheng, Droplet formation in a microfluidic T-junction involving highly viscous fluid systems, Chem. Eng. Sci. 145 (2016) 141–148.
[39] F. Scheiff, A. Holbach, D.W. Agar, Slug flow of ionic liquids in capillary microcontactors: fluid dynamic intensification for solvent extraction, Chem. Eng. Technol. 36 (2013) 975–984.
[40] J. Tan, J. Xu, S. Li, G. Luo, Drop dispenser in a cross-junction microfluidic device: scaling and mechanism of break-up, Chem. Eng. J. 136 (2008) 306–311.
[41] D. Tsaoulidis, P. Angeli, Effect of channel size on liquid-liquid plug flow in small channels, AIChE J. 62 (2016) 315–324.
[42] P. Garstecki, M.J. Fuerstman, H.A. Stone, G.M. Whitesides, Formation of droplets and bubbles in a microfluidic T-junction—scaling and mechanism of break-up, Lab Chip 6 (2006) 437–446.
[43] Q. Li, P. Angeli, Experimental and numerical hydrodynamic studies of ionic liquid-aqueous plug flow in small channels, Chem. Eng. J. 328 (2017) 717–736.
[44] Y. Su, G. Chen, Q. Yuan, Effect of viscosity on the hydrodynamics of liquid processes in microchannels, Chem. Eng. Technol. 37 (2014) 427–434.
[45] C. Yao, J. Zheng, Y. Zhao, Q. Zhang, G. Chen, Characteristics of gas-liquid Taylor flow with different liquid viscosities in a rectangular microchannel, Chem. Eng. J. 373 (2019) 437–445.
[46] S. Dharaskar, K.L. Wasewar, M.N. Varma, D.Z. Shende, C. Yoo, Synthesis, characterization and application of 1-butyl-3-methylimidazolium tetrafluoroborate for extractive desulfurization of liquid fuel, Arab. J. Chem. 9 (2013) 578–587.
[47] R.B. Bird, W.E. Stewart, E.N. Lightfoot, Transport Phenomena (2nd), Wiley, New Jersey, 2001.
[48] B. Susanti, J.G.M. Schuur, H.J. Winkelman, J. Heeres, Yue, Modelling studies of enantioselective extraction of an amino acid derivative in slug flow capillary microreactors, Chem. Eng. J. 354 (2018) 378–392.
[49] A. Ufer, D. Sudhoff, A. Mescher, D.W. Agar, Suspension catalysis in a liquid-liquid capillary microreactor, Chem. Eng. J. 167 (2011) 468–474.
[50] M.N. Kashid, A. Renken, L. Kiwi-Minsker, Gas-liquid and liquid-liquid mass transfer in microstructured reactors, Chem. Eng. Sci. 66 (2011) 3876–3897.
[51] C. Yao, H. Ma, Q. Zhao, Y. Liu, Y. Zhao, G. Chen, Mass transfer in liquid-liquid Taylor flow in a microchannel: local concentration distribution, mass transfer regime and the effect of fluid viscosity, Chem. Eng. Sci. 223 (2020), 115734.
[52] C. Yao, Y. Zhao, H. Ma, Y. Liu, Q. Zhao, G. Chen, Two-phase flow and mass transfer in microchannels: a review from local mechanism to global models, Chem. Eng. Sci. 229 (2021), 116017.
[53] N.D.M. Raimondi, L. Prat, C. Gourdon, J. Tasselli, Experiments of mass transfer with liquid-liquid slug flow in square microchannels, Chem. Eng. Sci. 105 (2014) 169–178.
[54] M. Kashid, I. Gerlach, S. Goetz, J. Franzke, J. Acker, F. Platte, D. Agar, S. Turek, Internal circulation within the liquid slugs of a liquid-liquid slug-flow capillary microreactor, Ind. Eng. Chem. Res. 44 (2005) 5003–5010.
[55] K. Wang, L. Li, P. Xie, G. Luo, Liquid-liquid microflow reaction engineering, React. Chem. Eng. 2 (2017) 611–627.
[56] J.B. Deshpande, A.A. Kulkarni, Effect of interfacial mass transfer on the dispersion in segmented flow in straight capillaries, AIChE J. 61 (2015) 4294–4308.